NASA/TM-2008-214635

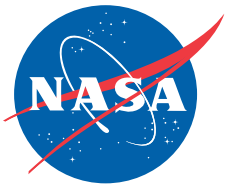

# Aeroservoelastic Stability Analysis of the X-43A Stack

*Chan-gi Pak*
*NASA Dryden Flight Research Center*
*Edwards, California*

**April 2008**

**NASA STI Program ... in Profile**

Since its founding, NASA has been dedicated to the advancement of aeronautics and space science. The NASA scientific and technical information (STI) program plays a key part in helping NASA maintain this important role.

The NASA STI program is operated under the auspices of the Agency Chief Information Officer. It collects, organizes, provides for archiving, and disseminates NASA's STI. The NASA STI program provides access to the NASA Aeronautics and Space Database and its public interface, the NASA Technical Report Server, thus providing one of the largest collections of aeronautical and space science STI in the world. Results are published in both non-NASA channels and by NASA in the NASA STI Report Series, which includes the following report types:

- TECHNICAL PUBLICATION. Reports of completed research or a major significant phase of research that present the results of NASA programs and include extensive data or theoretical analysis. Includes compilations of significant scientific and technical data and information deemed to be of continuing reference value. NASA counterpart of peer-reviewed formal professional papers but has less stringent limitations on manuscript length and extent of graphic presentations.

- TECHNICAL MEMORANDUM. Scientific and technical findings that are preliminary or of specialized interest, e.g., quick release reports, working papers, and bibliographies that contain minimal annotation. Does not contain extensive analysis.

- CONTRACTOR REPORT. Scientific and technical findings by NASA-sponsored contractors and grantees.

- CONFERENCE PUBLICATION. Collected papers from scientific and technical conferences, symposia, seminars, or other meetings sponsored or cosponsored by NASA.

- SPECIAL PUBLICATION. Scientific, technical, or historical information from NASA programs, projects, and missions, often concerned with subjects having substantial public interest.

- TECHNICAL TRANSLATION. English-language translations of foreign scientific and technical material pertinent to NASA's mission.

Specialized services also include creating custom thesauri, building customized databases, and organizing and publishing research results.

For more information about the NASA STI program, see the following:

- Access the NASA STI program home page at *http://www.sti.nasa.gov*

- E-mail your question via the Internet to help@sti.nasa.gov

- Fax your question to the NASA STI Help Desk at (301) 621-0134

- Phone the NASA STI Help Desk at (301) 621-0390

- Write to:
  NASA STI Help Desk
  NASA Center for AeroSpace Information
  7115 Standard Drive
  Hanover, MD 21076-1320

NASA/TM-2008-214635

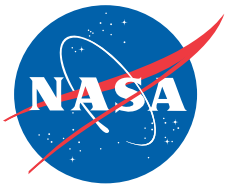

# Aeroservoelastic Stability Analysis of the X-43A Stack

*Chan-gi Pak*
*NASA Dryden Flight Research Center*
*Edwards, California*

National Aeronautics and
Space Administration

Dryden Flight Research Center
Edwards, California 93523-0273

**April 2008**

## NOTICE

Use of trade names or names of manufacturers in this document does not constitute an official endorsement of such products or manufacturers, either expressed or implied, by the National Aeronautics and Space Administration.

Available from:

NASA Center for AeroSpace Information
7115 Standard Drive
Hanover, MD 21076-1320
(301) 621-0390

## ABSTRACT

The first air launch attempt of an X-43A stack, consisting of the booster, adapter and Hyper-X research vehicle, ended in failure shortly after the successful drop from the National Aeronautics and Space Administration Dryden Flight Research Center (Edwards, California) B-52B airplane and ignition of the booster. The stack was observed to begin rolling and yawing violently upon reaching transonic speeds, and the grossly oscillating fins of the booster separated shortly thereafter. The flight then had to be terminated with the stack out of control. Very careful linear flutter and aeroservoelastic analyses were subsequently performed as reported herein to numerically duplicate the observed instability. These analyses properly identified the instability mechanism and demonstrated the importance of including the flight control laws, rigid-body modes, structural flexible modes and control surface flexible modes. In spite of these efforts, however, the predicted instability speed remained more than 25 percent higher than that observed in flight. It is concluded that transonic shock phenomena, which linear analyses cannot take into account, are also important for accurate prediction of this mishap instability.


## NOMENCLATURE

| | |
|---|---|
| AS | lateral acceleration |
| G | gain |
| HXRV | Hyper-X research vehicle |
| HXLV | Hyper-X launch vehicle |
| KEAS | knots equivalent airspeed |
| NASA | National Aeronautics and Space Administration |
| P | roll rate |
| Q | pitch rate |
| R | yaw rate |
| V-g | speed versus damping |
| V-ω | speed versus frequency |
| $\delta_L$ | left HXLV fin deflection angle |
| $\delta_R$ | right HXLV fin deflection angle |
| $\delta_V$ | vertical HXLV fin deflection angle |
| $\theta$ | pitch angle |
| $\phi$ | roll angle |
| $\psi$ | yaw angle |

## INTRODUCTION

The National Aeronautics and Space Administration (NASA) initiated the Hyper-X program in 1996 to explore hypersonic air-breathing propulsion and related technologies and to acquire flight data from scramjet engine performance for future vehicle design. The X-43A Hyper-X research vehicle (HXRV) was an air-launched scramjet vehicle designed to fly in the hypersonic flight regime and to be accelerated to its launching altitude and Mach number through the use of a conventional rocket booster designated the Hyper-X launch vehicle (HXLV). The HXRV was attached to the HXLV by way of the HXRV adapter, as shown in figure 1. This combination of the HXRV, the HXRV adapter, and the HXLV was designated the X-43A stack. For the X-43A, the HXLV was derived from a modified first stage of a Pegasus® (Pegasus is a registered trademark of Orbital Sciences Corporation, Dulles, Virginia) launch vehicle.

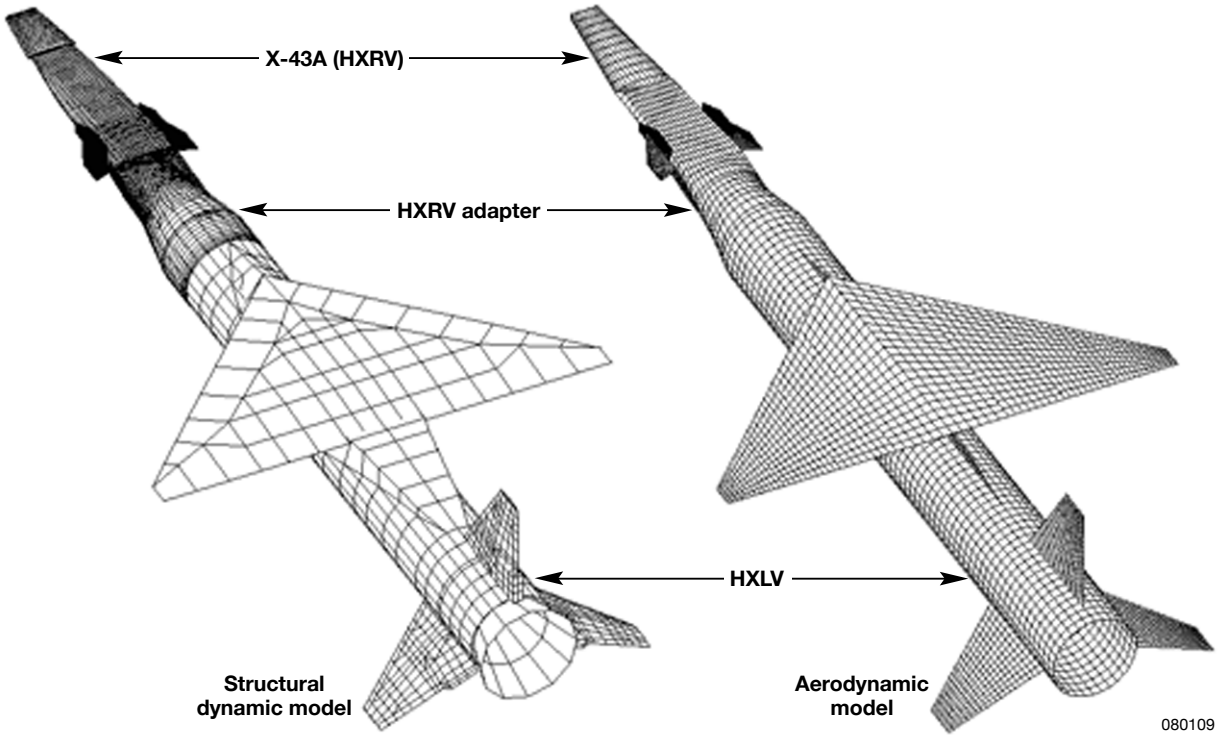


Figure 1. The X-43A stack.

The first X-43A HXRV flight attempt was conducted on June 2, 2001. The air-launched X-43A stack was carried by the NASA Dryden Flight Research Center (DFRC) (Edwards, California) B-52B airplane to an altitude of approximately 20 000 ft and released off the coast of California. Dynamic pressure at this altitude was higher than a typical Pegasus® launching. Ignition of the HXLV and a pitch-up maneuver of the X-43A stack took place approximately 5 s and 8 s, respectively, after release from the B-52B airplane. The HXLV was intended to accelerate the X-43A stack to the test altitude of 95 000 feet.

The X-43A mission profile is shown in figure 2. Approximately 11.5 s after release from the B-52B airplane, a control anomaly characterized by a diverging roll and yaw oscillation of the X-43A stack near 2 Hz developed at transonic speeds. These diverging oscillations caused the booster fins to separate nearly 13 s after release, and the out-of-control vehicle was terminated (ref. 1).

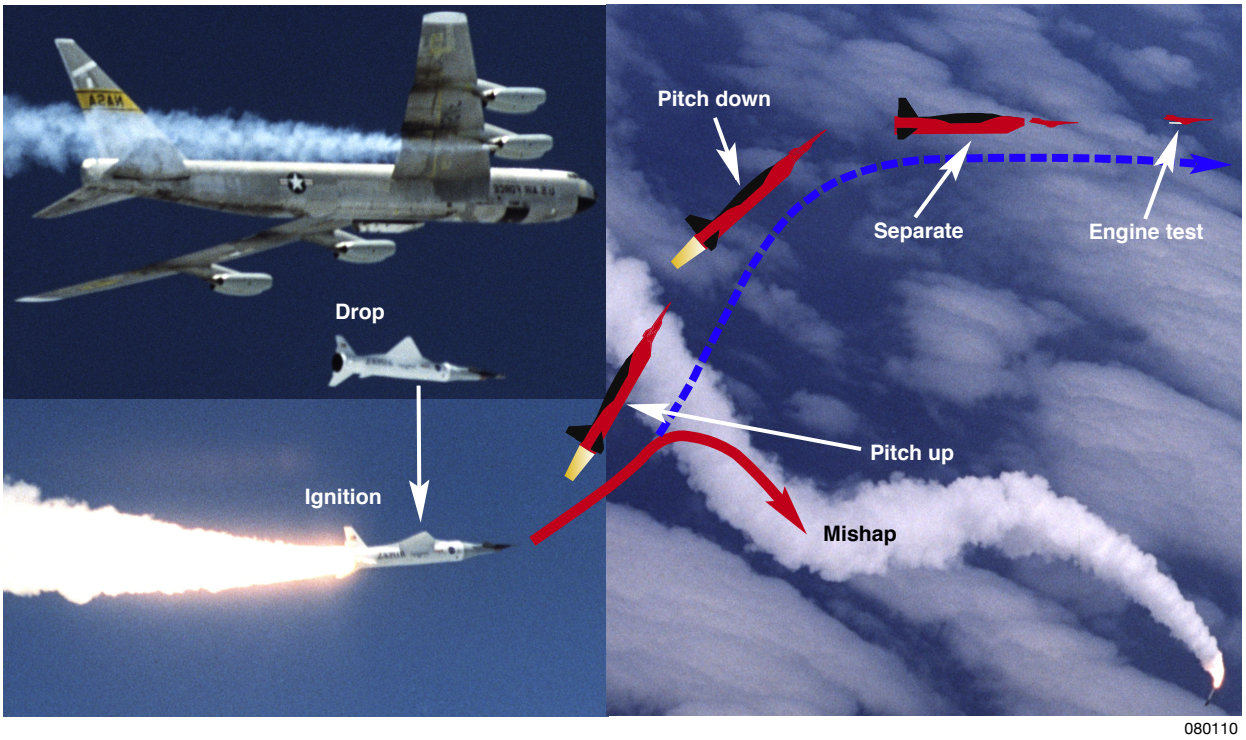


Figure 2. The X-43A mission profile.

In an attempt to predict the first flight instability of the X-43A stack, an independent investigation was performed using linear aeroelastic and aeroservoelastic analyses at the NASA Dryden Flight Research Center. Anti-symmetric low frequency motions, such as rolling and yawing oscillations, that were evident just prior to the loss of control, necessitated more realistic surface representation than was provided by the previous aerodynamic model. Additional modeling features that were employed here, but not previously utilized, were cylindrical body aerodynamic paneling, the mean flow effect, and atmospheric matched point solutions. The observed oscillatory commands to the stack fins before the failure would press the need to include the X-43A stack flight control laws for an aeroservoelastic analysis.

The aeroelastic approach alone predicted an open-loop flutter velocity well above that of the flight mishap, however, the corresponding flutter frequency matched precisely with what was observed. When the stack flight control laws were implemented in the aeroservoelastic stability analysis, considerable improvement in the predicted instability velocity was achieved.

## TRIM ANALYSIS

The ZAERO code (ref. 2) (ZONA Technology, Incorporated, Scottsdale, Arizona), based on a harmonic gradient method, was used for the aeroelastic and aeroservoelastic computer simulations. The detailed aerodynamic model geometry, including 6076 box divisions, can be seen in figure 1. The slender body effects of the HXLV and HXRV were included in this aerodynamic model. The fairing between the HXLV wing and body was idealized using vertical aerodynamic boxes, since some distance between the centerline elements along the HXLV wing and body are required to overcome numerical difficulties.

During the pull-up maneuver, the X-43A stack experienced nonzero angle of attack, sideslip angle, and booster fin deflection angles. These nonzero angles can reduce flutter speed especially in transonic flight regime. The mean flow effects due to the nonzero angles were included in the open- and closed-loop flutter analyses. The mean flow conditions were computed using asymmetric trim analysis.

The MSC Software (Santa Ana, California) MSC Nastran code (ref. 3) was used to generate the natural frequencies and mode shapes of the structure, which served as input for the open- and closed-loop flutter analyses using the ZAERO code ZONA6 for subsonic applications. The Lanczos eigensolver was selected for the MSC Nastran modal analysis, and a finite element model is shown in figure 1. A total of 66 structural modes (6 rigid-body and 60 flexible) were used for the ZAERO computations.

Structural responses and aerodynamic pressures are coupled in an aeroelastic analysis through the use of the interpolation points, and the selection of good interpolation points is one of the most important factors for a successful aeroelastic analysis. Good or bad interpolation points can be checked with interpolated mode shapes on the aerodynamic model. Selected mode shapes are shown in figures 3 and 4.

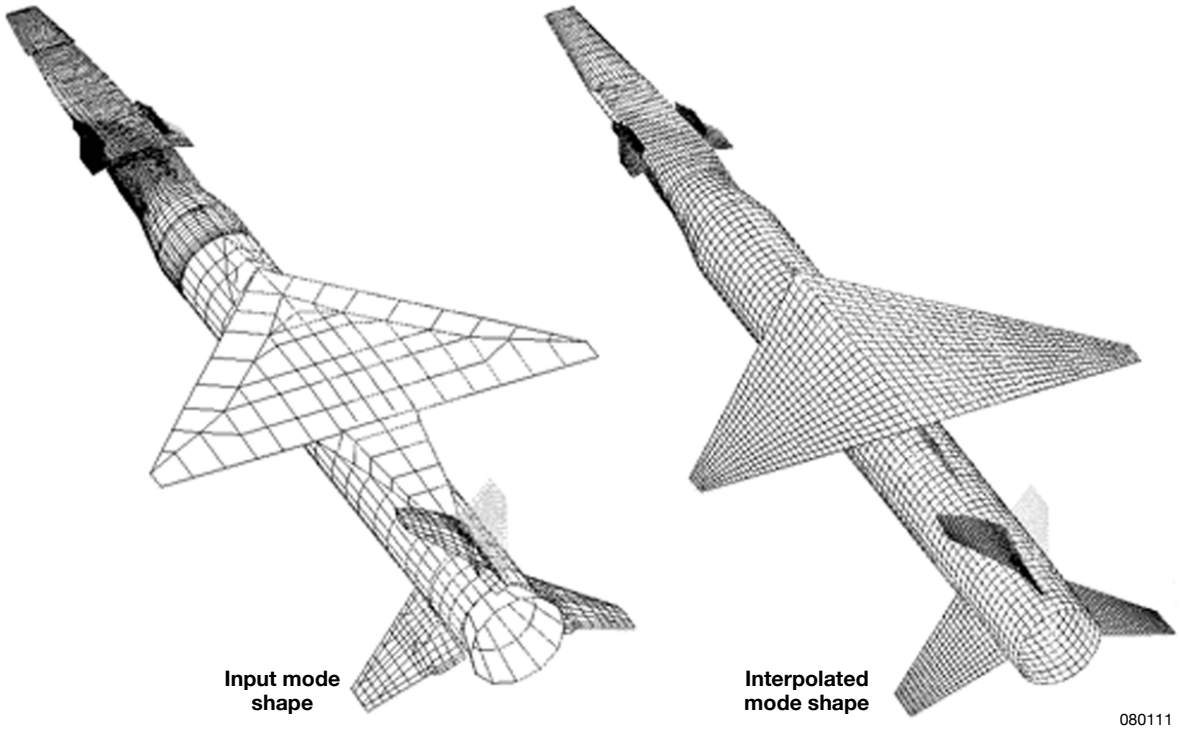


Figure 3. Vertical Hyper-X launch vehicle fin bending: 13.67 Hz (11th structural mode).

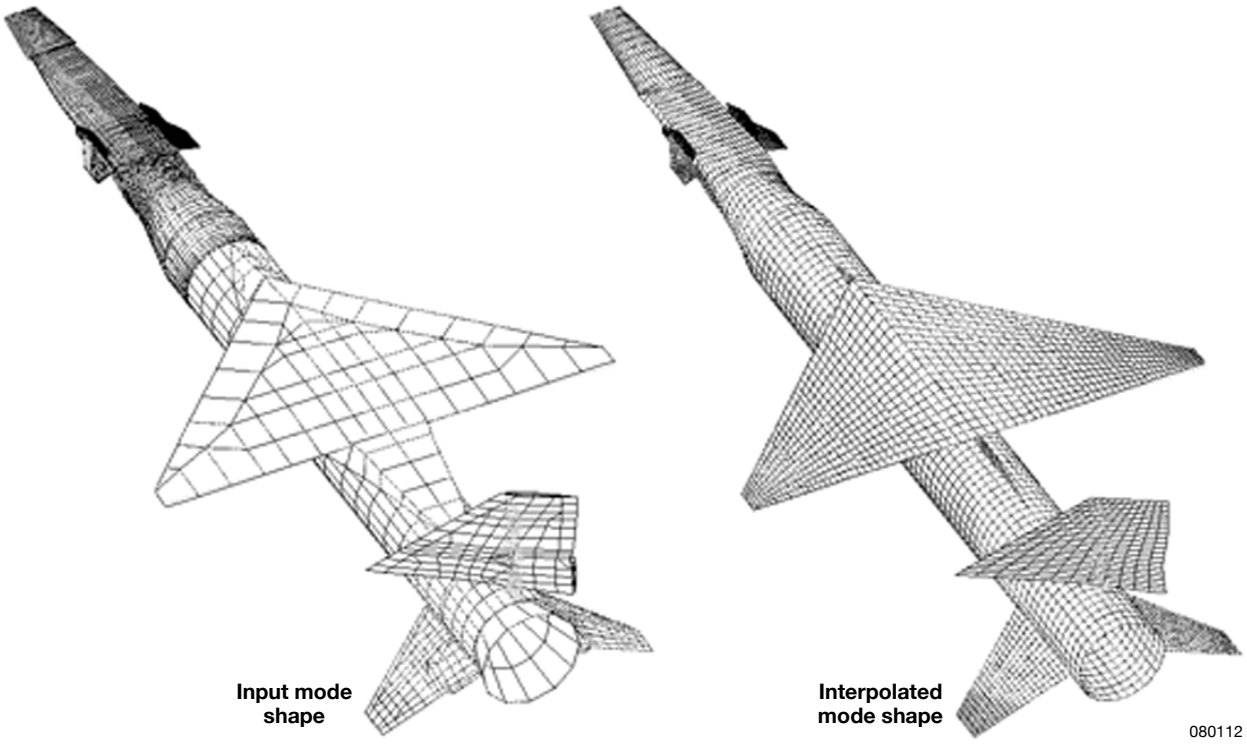


Figure 4. Vertical Hyper-X launch vehicle fin actuator rotation: 27.93 Hz (23rd structural mode).

A trim analysis had been performed to include the mean flow effects in both the open- and closed-loop flutter analyses, therefore, the unsteady aerodynamics for the flutter analysis were coupled with the steady mean flow aerodynamics. The mean flow conditions included angle of attack, sideslip angle, roll, pitch, and yaw rates, and the HXLV fin deflection angles.

The trim analysis was performed at a Mach number of 0.9, and input data and output results are summarized in table 1. Five trim degrees of freedom were all measured during the first X-43A stack flight. The HXLV fin deflection angles computed using linear subsonic theory were approximately 25 percent smaller than those measured at the transonic flight condition. Corresponding pressure coefficients are shown in figure 5.

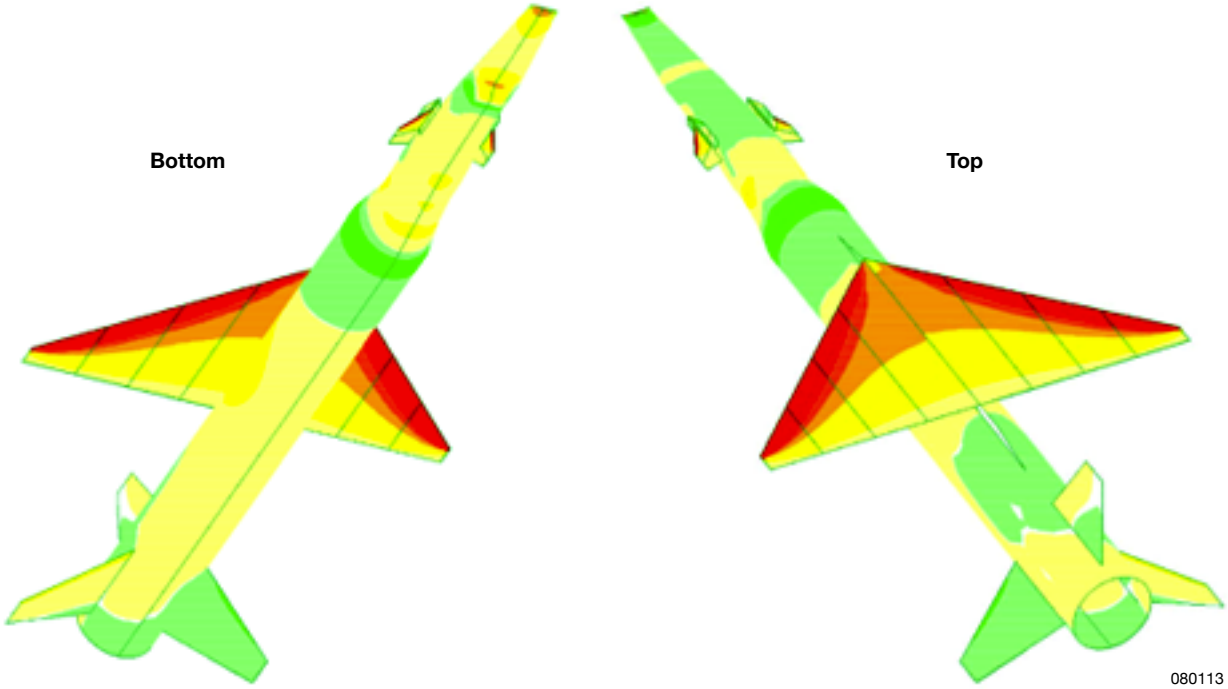


Figure 5. Pressure coefficients at trim condition.

Table 1. Trim conditions at Mach 0.9 and an altitude of 22 530 ft.

| | ZAERO trim input | Measured |
|---|---|---|
| Roll acceleration | 0.0°/s$^2$ | 0.0°/s$^2$ |
| Pitch acceleration | 0.0°/s$^2$ | 1.30°/s$^2$ |
| Yaw acceleration | 0.0°/s$^2$ | -5.00°/s$^2$ |
| Roll rate | 0.0°/s | 2.09°/s |
| Pitch rate | 0.0°/s | 1.75°/s |
| Yaw rate | 0.0°/s | 0.12°/s |
| Angle of attack | 12.44° | 12.44° |
| Side slip angle | -0.22° | -0.22° |
| | ZAERO trim results | Measured |
| $\delta_R$: right fin angle | -8.442° | -11.14° |
| $\delta_L$: left fin angle | -8.531° | -10.77° |
| $\delta_V$: vertical fin angle | -0.2794° | -1.397° |
| $N_y$ acceleration | 2.0 in/s$^2$ | 12.0 in/s$^2$ |
| $N_z$ acceleration | 616.56 in/s$^2$ | 518.76 in/s$^2$ |

## OPEN-LOOP FLUTTER ANALYSIS

Flutter analysis of the X-43A stack during the first flight using the ZAERO code is presented in this section. The subsonic aerodynamic model for the trim analysis, shown in figure 1, was also used for the flutter analysis. The aerodynamic influence coefficient matrices were generated at 16 reduced frequencies and the g-method (ref. 2) was used in the matched flutter analysis.

The matched flutter analyses with the mean flow condition were performed at Mach 0.9 and an altitude of 22 530 ft. The speed versus damping, V-g, and speed versus frequency, V-ω, curves from the open-loop flutter analysis with mean flow effect are shown in figure 6, and a summary of flutter boundaries with and without mean flow effects is shown in table 2. A maximum error of 1.7 percent in the flutter frequency is observed in the table 2 data. From the data shown in table 2, we may conclude that the mean flow effects are negligibly small.

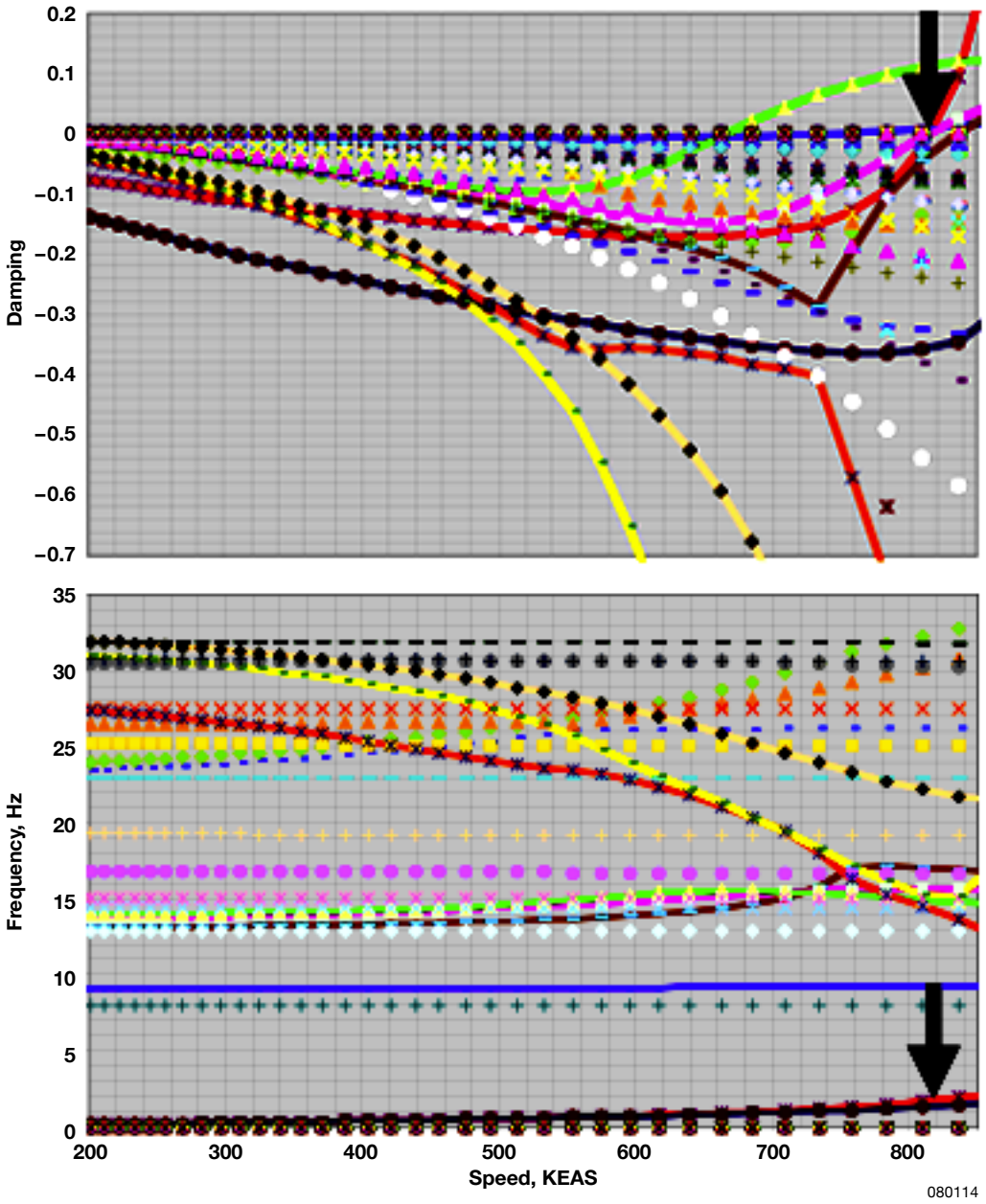


Figure 6. Open-loop flutter analysis with mean flow effect at Mach = 0.9.

Table 2. Mean flow effects on open-loop flutter boundaries at Mach 0.9 and an altitude of 22 530 ft.

| Flutter mode | Flutter speed, KEAS | | | Flutter frequency, Hz | | |
|---|---|---|---|---|---|---|
| | With | Without | Difference, % | With | Without | Difference, % |
| 1 | 667 | 667 | 0.0 | 15.5 | 15.5 | 0.0 |
| 2 | 754 | 746 | 1.1 | 9.27 | 9.27 | 0.0 |
| 3 | 815 | 813 | 0.2 | 1.78 | 1.75 | 1.7 |
| 4 | 816 | 815 | 0.1 | 15.7 | 15.7 | 0.0 |
| 5 | 835 | 836 | -0.1 | 16.9 | 16.9 | 0.0 |

It should be noted that huge rigid-body yaw and roll motions together with the flexible HXLV fin motions were actually observed just before the mishap of the first flight. The frequency of this mishap motion was approximately 2 Hz. The third flutter speed shown in table 2 is 815 knots equivalent airspeed (KEAS), and this speed is far from the actual flight speed of 383 KEAS. We should notice, however, that the third flutter frequency of 1.78 Hz was predicted through the use of the linear analysis. The third flutter mode shape and modal participation factors are given in figure 7 and table 3, respectively. Rigid yaw motion can be easily observed in the top view, and rigid roll motion can be observed in the rear view. The vertical HXLV fin actuator rotation and the flexible fin bending motion were coupled with rigid yaw and roll motion. In table 3, 33 percent and 65 percent of the flutter motion are from the rigid and flexible modes, respectively. It is quite interesting that the rigid pitch was not involved in this flutter mode. There is no noticeable pitch motion in the side view of the flutter mode shape shown in figure 7.

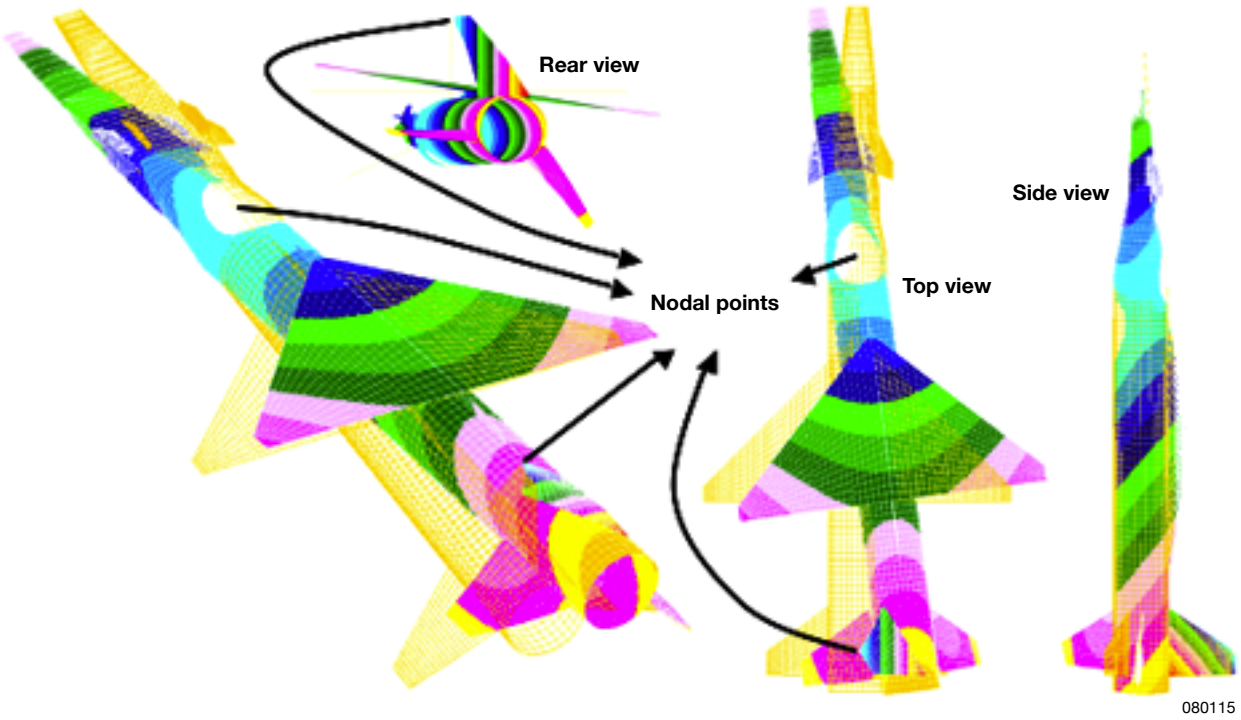


Figure 7. The third flutter mode shape: flutter frequency 1.78 Hz; flutter speed 815 KEAS.

Table 3. Modal participation factors for the third flutter mode.

| Structural mode | Modal participation, % | | Description |
|---|---|---|---|
| 2 | 2.6 | | Rigid lateral |
| 4 | 0.2 | 32.7 | Rigid roll |
| 6 | 29.9 | | Rigid yaw |
| 8 | 2.3 | | First lateral bending of X-43A stack |
| 10 | 3.8 | | Right HXLV fin first bending |
| 11 | 14.3 | | Vertical HXLV fin first bending |
| 12 | 2.1 | | Left HXLV fin first bending |
| 21 | 0.5 | 65.4 | First HXRV and adapter torsion |
| 23 | 29.8 | | Vertical HXLV fin actuator rotation |
| 24 | 0.2 | | Right and left HXLV fin actuators rotation and fins bending |
| 26 | 6.4 | | Right HXLV fin actuator rotation |
| 28 | 2.6 | | Left HXLV fin actuator rotation |
| 54 | 3.3 | | Vertical, right, and left HXLV fins second bending |
| other | 1.9 | | |

## CLOSED-LOOP AEROSERVOELASTIC STABILITY ANALYSIS

A block diagram of the flight control system used for the closed-loop flutter analysis is shown in figure 8. Sensor dynamics, control law, and actuator dynamics are included in the closed-loop flutter analysis. The gain scheduling was used to adapt aeroelastic system changes during the actual flight. Gain values at the Mach 0.9 condition were selected for the closed-loop flutter analysis with the symmetric and anti-symmetric control laws fully coupled.

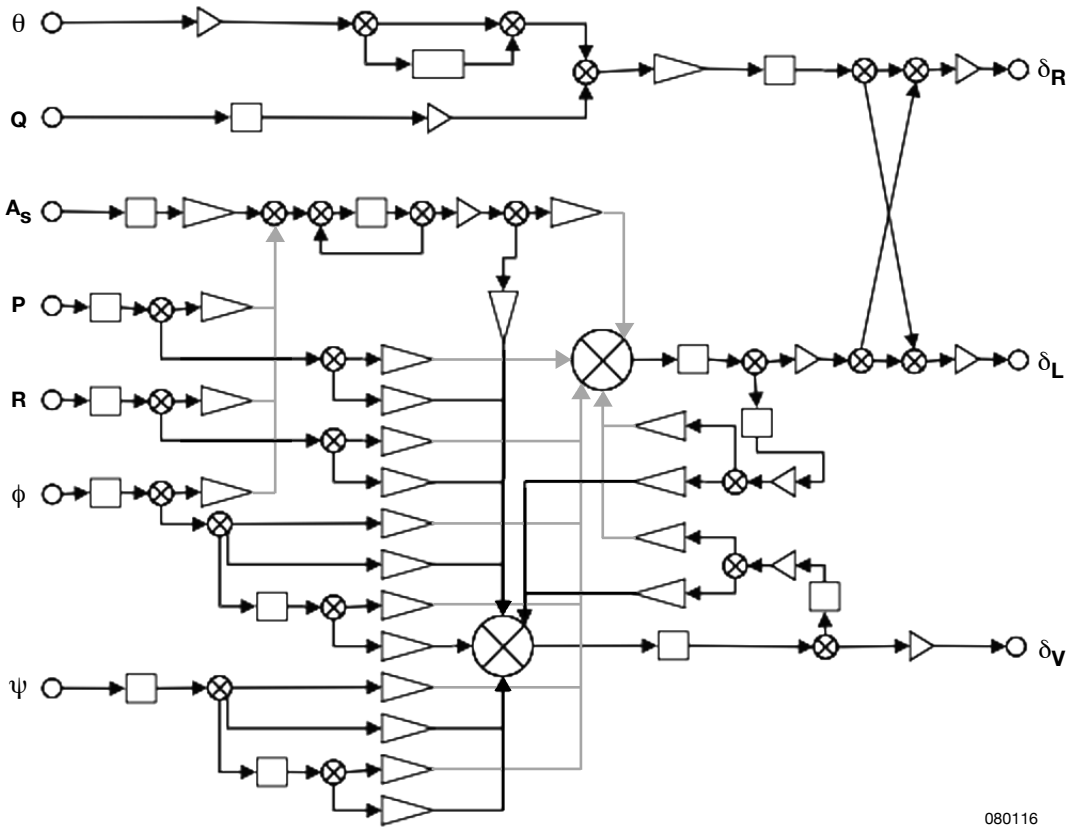


Figure 8. Block diagram of the X-43A flight control system.

The V-g and V-ω curves from the closed-loop flutter analysis are shown in figure 9. This figure shows an instability occurring at M = 0.9 and V = 508 KEAS. The flutter frequency associated with this instability is approximately 1.39 Hz. The primary flutter mode shown here was the same third flutter mode that was shown in figure 6. The flutter speed of this mode was drastically decreased from 815 KEAS to 508 KEAS and the corresponding flutter frequency was changed from 1.78 Hz to 1.39 Hz as shown in tables 2 and 4. It should be noted with regard to figure 9 that the predicted flutter speed was decreased 71 percent because of the coupling between the aeroelastic structure and the control system.

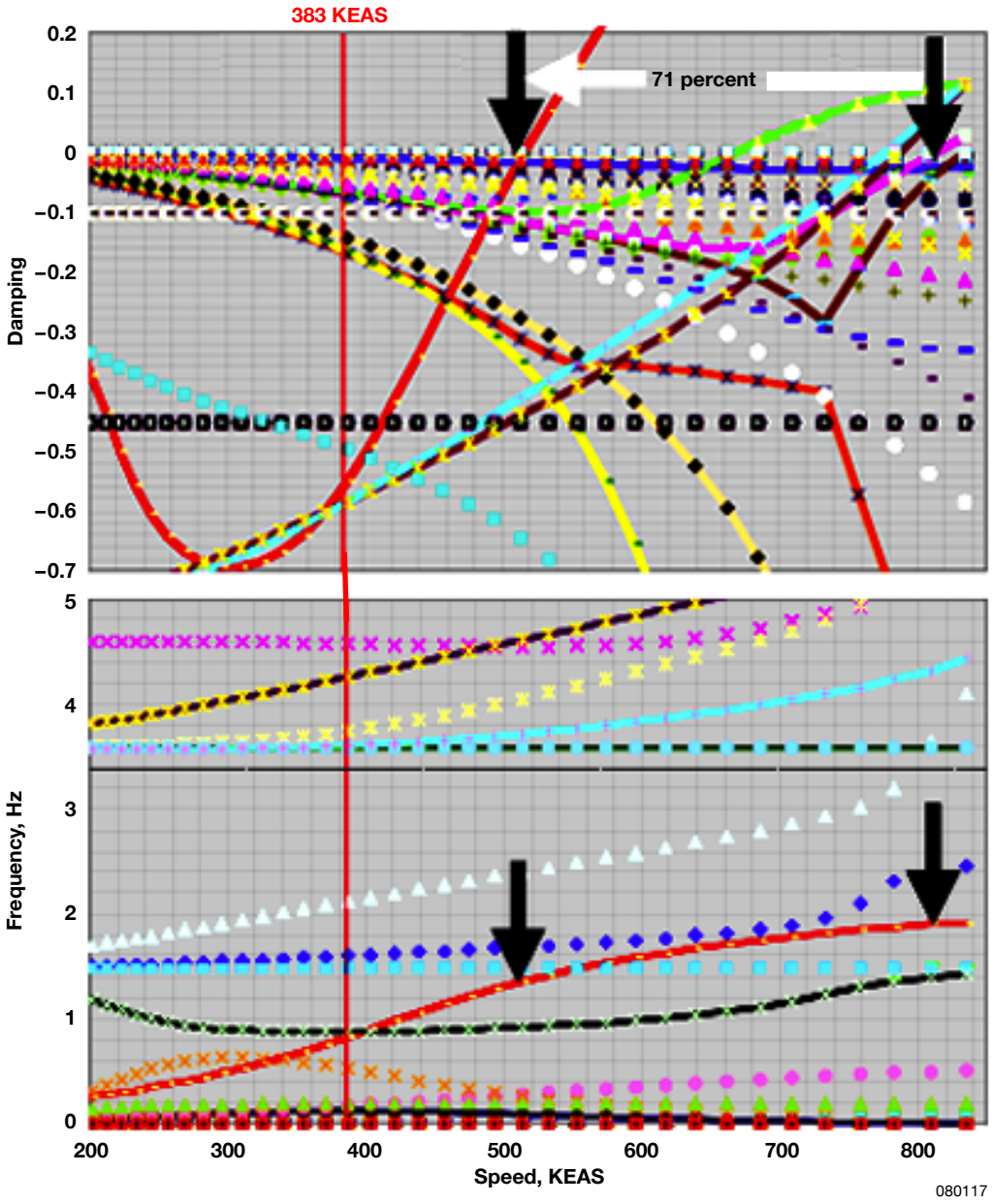


Figure 9. Closed-loop flutter analysis at Mach = 0.9.

Table 4. Vertical fin effectiveness study, G = gain.

| Flutter mode | Flutter speed, KEAS | | | | | | | Flutter frequency, Hz | | | | | | |
|---|---|---|---|---|---|---|---|---|---|---|---|---|---|---|
| | G=1 | 1.75 | 2.00 | 2.25 | 2.50 | 3.00 | 3.80 | G=1 | 1.75 | 2.00 | 2.25 | 2.50 | 3.00 | 3.80 |
| 1 | 508 | 478 | 470 | 460 | 449 | 422 | 368 | 1.39 | 1.75 | 1.86 | 1.98 | 2.08 | 2.27 | 2.44 |
| 2 | 668 | 669 | 666 | 652 | 641 | 628 | 628 | 15.5 | 15.5 | 3.77 | 3.68 | 3.59 | 3.43 | 3.43 |
| 3 | 772 | 684 | 669 | 669 | 669 | 669 | 669 | 3.87 | 3.86 | 15.5 | 15.5 | 15.5 | 15.5 | 15.5 |
| 4 | 792 | 769 | 758 | 747 | 736 | 716 | 716 | 5.22 | 5.69 | 5.80 | 5.88 | 5.96 | 6.08 | 6.08 |
| 5 | 811 | 808 | 807 | 806 | 805 | 803 | 803 | 15.7 | 15.7 | 15.7 | 15.7 | 15.6 | 15.6 | 15.6 |
| 6 | 837 | 837 | 838 | 838 | 838 | 838 | 838 | 16.9 | 16.9 | 16.9 | 16.9 | 16.9 | 16.9 | 16.9 |
| 7 | 1010 | 1070 | 1090 | 1110 | 1120 | 1150 | 1150 | 9.41 | 9.49 | 9.52 | 9.55 | 9.58 | 9.64 | 9.64 |

A vertical fin effectiveness study was also performed in the current investigation. The aeroservoelastic instability mechanism is mainly an interaction between the structural rigid-body yaw, vertical fin actuator rotation, vertical fin first bending, and flight control modes. When the gain values are smaller than 2.5, the structural mode is the critical one; however, when the gain values are larger than 2.5, the flight control mode becomes the more critical one. Flutter speeds and frequencies based on different gain values are summarized in table 4. When gain values are increased, the flutter speeds and frequencies approach the mishap speeds and frequencies, respectively.

A flutter analysis with only the rigid-body and the flight control modes but not the structural flexible modes was also performed to verify the role of elastic effects on the closed-loop flutter mode. The V-g and V-ω curves are shown in figure 10. The flutter speed was increased from 508 KEAS to 568 KEAS while the corresponding flutter frequency was unchanged. The predicted primary flutter speed was erroneously increased 32 percent, demonstrating the importance of including the elastic modes. Flutter boundaries are summarized in figure 11.

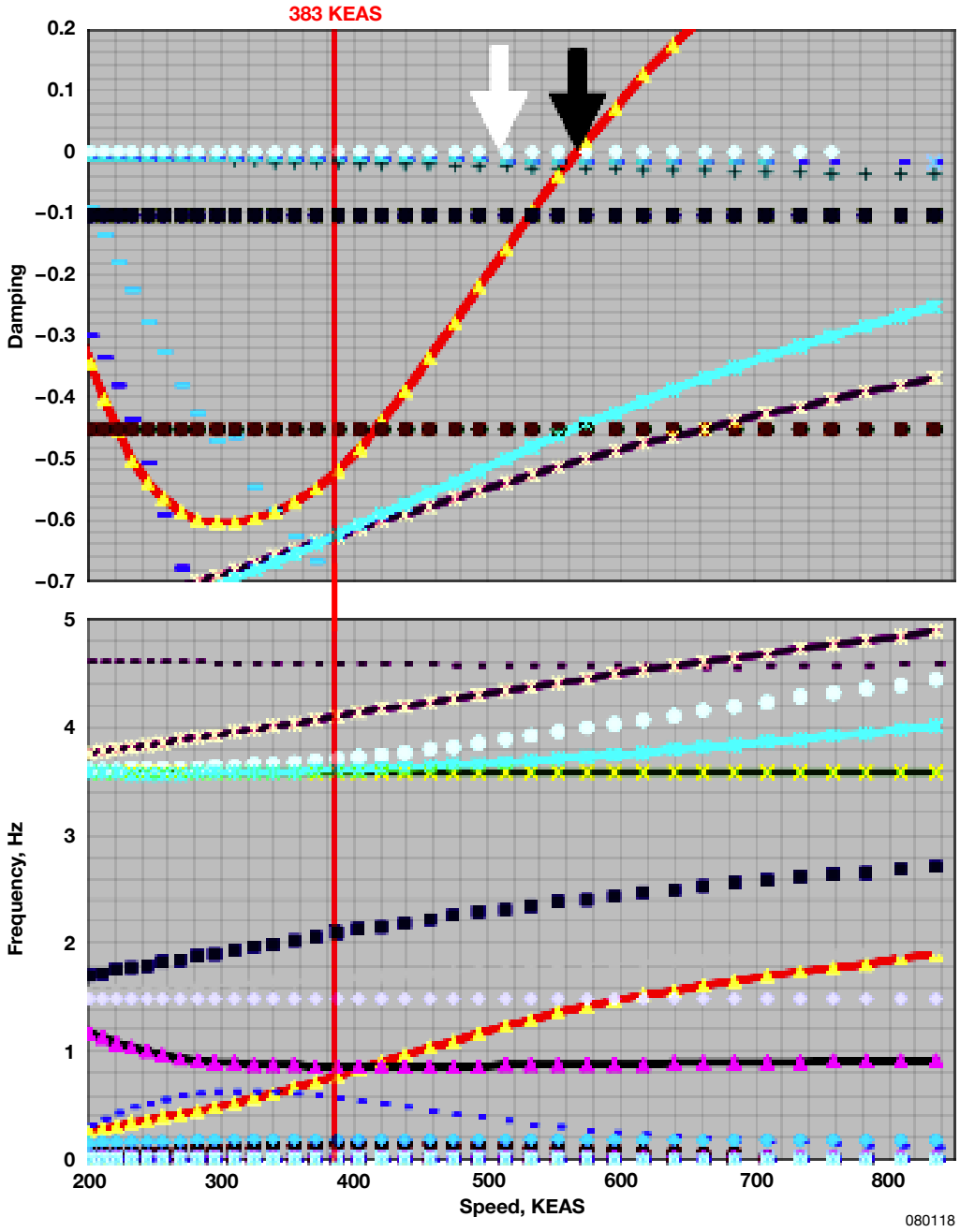


Figure 10. Closed-loop flutter analysis at Mach = 0.9 with rigid structural modes.

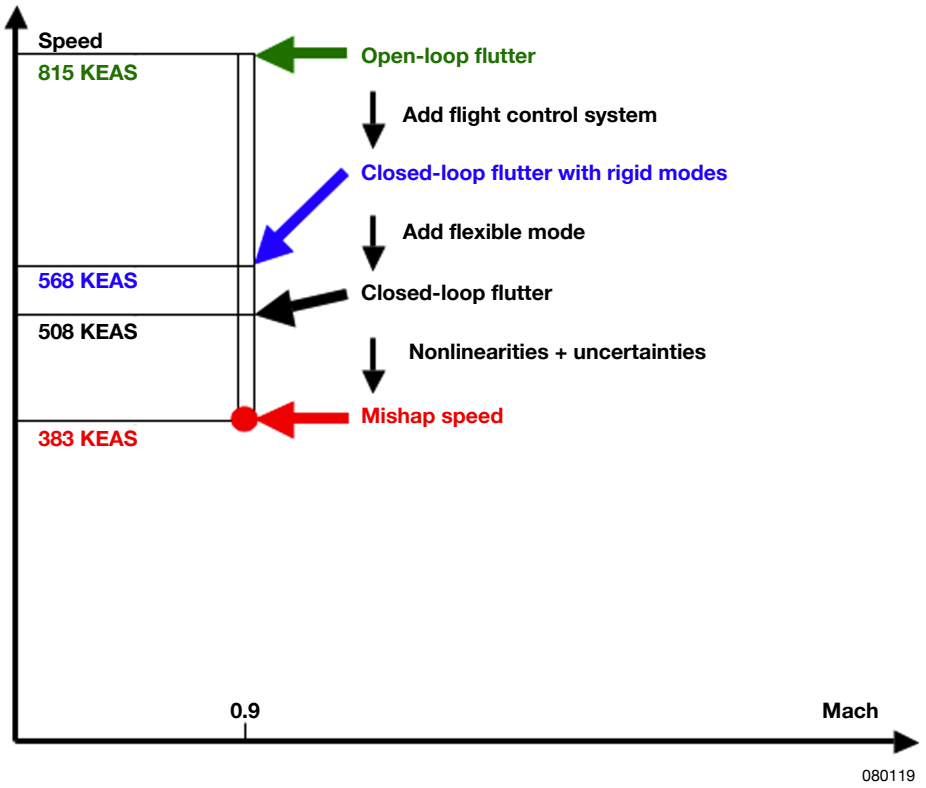


Figure 11. Summary of flutter boundaries.

## CONCLUSION

Improved aerodynamic and flight control models were used for the open- and closed-loop flutter analyses. The anti-symmetric failure mode, at 1.92 Hz, was successfully captured, however, the corresponding predicted flutter speed was still too high. To improve the accuracy of the flutter speed and frequency prediction, we may consider the nonlinear transonic effects. Flutter speed in the transonic flight regime can be drastically decreased due to embedded shocks. A computational fluid dynamics-based transonic flutter analysis was performed at the National Aeronautics and Space Administration Langley Research Center, Hampton, Virginia, using Computational Fluids Laboratory-3D (CFL3D) Navier-Stokes simulations. Because of a negative volume problem during unsteady aeroelastic computations, however, this work was not successful (private communication with Dave Schuster).

The mishap of the first X-43A stack flight was caused by the anti-symmetric body freedom flutter which was an interaction between the rigid-body yaw, vertical fin actuator rotation, vertical fin first bending, and flight control modes. Therefore, the following updates and changes were the correct actions for the second and third X-43A stack flights that could change the characteristics of the anti-symmetric body freedom flutter and improve the flutter prediction: updating the aerodynamic model (especially the anti-symmetric model); changing the moment of inertia of the Pegasus® (Pegasus is a registered trademark of Orbital Sciences Corporation, Dulles, Virginia) rocket booster; stiffening the fin actuators; and updating the flight control model.

## REFERENCES


1. X-43A Mishap Investigation Board, "Report of Findings X-43A Mishap," Volume I, 2003.

2. ZONA Technology, Inc., *ZAERO User's Manual Engineer's Toolkit for Aeroelastic Solutions*, ZONA Technology, Inc., 2007.

3. Reymond, Michael and Mark Miller, eds., *MSC/NASTRAN Quick Reference Guide Version 69*, The MacNeal-Schwendler Corporation, USA, 1996.

# REPORT DOCUMENTATION PAGE

*Form Approved*
*OMB No. 0704-0188*



| 1. REPORT DATE *(DD-MM-YYYY)* | 2. REPORT TYPE | 3. DATES COVERED *(From - To)* |
|---|---|---|
| 01-04-2008 | Technical Memorandum | |

**4. TITLE AND SUBTITLE**
Aeroservoelastic Stability Analysis of the X-43A Stack

**5a. CONTRACT NUMBER**

**5b. GRANT NUMBER**

**5c. PROGRAM ELEMENT NUMBER**

**6. AUTHOR(S)**
Pak, Chan-gi

**5d. PROJECT NUMBER**

**5e. TASK NUMBER**

**5f. WORK UNIT NUMBER**

**7. PERFORMING ORGANIZATION NAME(S) AND ADDRESS(ES)**
NASA Dryden Flight Research Center
P.O. Box 273
Edwards, California 93523-0273

**8. PERFORMING ORGANIZATION REPORT NUMBER**
H-2837

**9. SPONSORING/MONITORING AGENCY NAME(S) AND ADDRESS(ES)**
National Aeronautics and Space Administration
Washington, DC 20546-0001

**10. SPONSORING/MONITOR'S ACRONYM(S)**
NASA

**11. SPONSORING/MONITORING REPORT NUMBER**
NASA/TM-2008-214635

**12. DISTRIBUTION/AVAILABILITY STATEMENT**
Unclassified -- Unlimited
Subject Category 08 Availability: NASA CASI (301) 621-0390 Distribution: Standard

**13. SUPPLEMENTARY NOTES**
Pak, NASA Dryden Flight Research Center. An electronic version can be found at http://dtrs.dfrc.nasa.gov or http://ntrs.nasa.gov/search.jsp.

**14. ABSTRACT**

The first air launch attempt of an X-43A stack, consisting of the booster, adapter and Hyper-X research vehicle, ended in failure shortly after the successful drop from the National Aeronautics and Space Administration Dryden Flight Research Center (Edwards, California) B-52B airplane and ignition of the booster. The stack was observed to begin rolling and yawing violently upon reaching transonic speeds, and the grossly oscillating fins of the booster separated shortly thereafter. The flight then had to be terminated with the stack out of control. Very careful linear flutter and aeroservoelastic analyses were subsequently performed as reported herein to numerically duplicate the observed instability. These analyses properly identified the instability mechanism and demonstrated the importance of including the flight control laws, rigid-body modes, structural flexible modes and control surface flexible modes. In spite of these efforts, however, the predicted instability speed remained more than 25 percent higher than that observed in flight. It is concluded that transonic shock phenomena, which linear analyses cannot take into account, are also important for accurate prediction of this mishap instability.

**15. SUBJECT TERMS**
Body freedom flutter, Closed-loop flutter, Mishap instability, Open-loop flutter, X-43A stack

| 16. SECURITY CLASSIFICATION OF: | | | 17. LIMITATION OF ABSTRACT | 18. NUMBER OF PAGES | 19b. NAME OF RESPONSIBLE PERSON |
|---|---|---|---|---|---|
| a. REPORT | b. ABSTRACT | c. THIS PAGE | | | STI Help Desk (email: help@sti.nasa.gov) |
| | | | | | 19b. TELEPHONE NUMBER *(Include area code)* |
| U | U | U | UU | 21 | (301) 621-0390 |